Chemical Science

ROYAL SOCIETY OF CHEMISTRY

EDGE ARTICLE

View Article Online
View Journal | View Issue

Cite this: *Chem. Sci.*, 2025, **16**, 9785

All publication charges for this article have been paid for by the Royal Society of Chemistry

Received 1st January 2025
Accepted 24th April 2025

DOI: 10.1039/d5sc00003c

rsc.li/chemical-science

Vacuum evaporation-assisted reaction: sustainable solution for application of rare earth-based halide solid-state electrolytes†

Zhichao Zeng, Xiaomeng Shi, Hongtu Zhang and Yaping Du *

All-solid-state lithium-ion batteries (ASLIBs) are important and promising electric energy storage devices with high stabilities and energy densities. As burgeoning key materials in ASLIBs, rare earth (RE) halide solid-state electrolytes (SEs) have better overall electrochemical performance than do oxide and sulfide SEs. Technologies for the efficient preparation, mass production and recycling of RE halide SEs (HSEs) are challenges that urgently need to be overcome. In this study, products and byproducts can be separated in an orderly manner *via* a vacuum evaporation-assisted reactor for the green synthesis of 15 kinds of RE HSEs and nine kinds of RE halide perovskites. The as-prepared HSEs have high ionic conductivities (mS cm^{-1} level) and wide electrochemical windows (1.4–4.2 V). The assembled Li–S ASLIBs were stable for up to 550 cycles. This work realized massive preparation and recycling of RE HSEs and crucial metal resources.

Introduction

All-solid-state lithium-ion batteries (ASLIBs) possess high safety and energy density, so studies on the key materials and technologies of ASLIBs have become a hot topic.[1–4] Solid-state electrolytes (SEs) are among the most important materials supporting the development of ASLIBs.[5–7] Rare earth (RE) halide SEs (HSEs) have many advantages, such as high lithium-ion conductivity, high oxidation stability, good cold deformability, and high oxygen and heat stability, and have great application potential in ASLIBs.[8–14] Mechanochemical ball-milling (BM) and co-melting (CM) methods are commonly used to prepare HSEs (Li_3REX_6, RE = Sc, Y, Gd–Lu; X = Cl, Br), which are energy-intensive and time consuming, expensive anhydrous halide salts (LiX and REX_3) are needed, and the processes must react in an inert gas atmosphere to prevent salts deliquescence (eqn (1) and (2)).[15–19] Therefore, new methods for the high-efficiency, low-cost and convenient preparation of HSEs are urgently needed.[20–23] In addition, lithium and RE metals are non-renewable resources, so the cycling and reuse technologies of RE HSEs are important for the sustainable development of ASLIBs.[24–28] To obtain more reasonable, energy-saving and environmentally friendly chemical technologies, it is necessary to integrate the green chemistry criteria into the process of RE HSEs preparation and recycling.[29–33]

Notably, the melting and boiling points of RE and lithium halides are higher than the sublimation points of NH_4Cl (338 °C) and NH_4Br (396 °C) (Table S1†), and NH_4X with low heat stability can split into NH_3 and HX gases at high temperature, and return to solid NH_4X at low temperature (eqn (3) and (4)). The HX gas from NH_4X can react with metal oxygen-containing compounds ($REX_3 \cdot nH_2O$, REOX, RE_2O_3, LiOH, Li_2CO_3, *etc.*) to form solid anhydrous halide salts (REX_3 and LiX), H_2O vapor and CO_2. Therefore, anhydrous REX_3 and LiX can be prepared or purified *via* the ammonium halide (NH_4X) sublimation-assisted method (eqn (5) and (6)).[34,35] During this process, the NH_3, HX and H_2O gases can be removed from the reactor under vacuum (eqn (7)–(10)).[36,37] If certain proportions of anhydrous lithium and RE halides are purified simultaneously, the mixture of LiX and REX_3 will form RE HSEs at high temperature.[38–41] This is an optimal reaction process for the synthesis of HSEs, and the products of Li_3REX_6, sublimable NH_4X, and other impurities (the gases of CO_2, NH_3, and H_2O) can be well separated and removed.

$$REX_3 + nH_2O \rightarrow REX_3 \cdot nH_2O \quad (1)$$

$$LiX + mH_2O \rightarrow LiX \cdot mH_2O \quad (2)$$

$$NH_4X \xrightarrow{\Delta} NH_3\uparrow + HX\uparrow \quad (3)$$

$$NH_3\uparrow + HX\uparrow \xrightarrow{\text{cooling}} NH_4X \quad (4)$$

$$REX_3 \cdot nH_2O \xrightarrow{\Delta/NH_4X} REX_3 + nH_2O\uparrow \quad (5)$$

Tianjin Key Lab for Rare Earth Materials and Applications, Center for Rare Earth and Inorganic Functional Materials, Haihe Laboratory of Sustainable Chemical Transformations, Smart Sensing Interdisciplinary Science Center, School of Materials Science and Engineering, National Institute for Advanced Materials, Nankai University, Tianjin 300350, China. E-mail: ypdu@nankai.edu.cn

† Electronic supplementary information (ESI) available. See DOI: https://doi.org/10.1039/d5sc00003c

$$LiX\cdot mH_2O \xrightarrow{\Delta/NH_4X} LiX + mH_2O\uparrow \quad (6)$$

$$RE_2(CO_3)_3 + 6NH_4X \xrightarrow{\Delta/NH_4X} 2REX_3 + 3H_2O\uparrow + 3CO_2\uparrow + 6NH_3\uparrow \quad (7)$$

$$RE_2O_3 + 6NH_4X \xrightarrow{\Delta/NH_4X} 2REX_3 + 3H_2O\uparrow + 6NH_3\uparrow \quad (8)$$

$$REOX + 2NH_4X \xrightarrow{\Delta/NH_4X} REX_3 + H_2O\uparrow + 2NH_3\uparrow \quad (9)$$

$$Li_2CO_3 + 2NH_4X \xrightarrow{\Delta/NH_4X} 2LiX + H_2O\uparrow + CO_2\uparrow + 2NH_3\uparrow \quad (10)$$

On the basis of the above concept, this work uses a vacuum evaporation-assisted (VEA) reactor to green prepare and recycle RE HSEs. This VEA reactor can be used to massively prepare RE HSEs by using inexpensive RE oxides (or carbonates) and lithium carbonate as the raw materials. Moreover, RE halide materials can be prepared in this way. During halides preparation, almost all the chemicals can be recycled, and closed-loop circulation was realized. The prepared RE HSEs have high ionic conductivity (~1 mS cm^{-1}), excellent deformability and intimate contact with electrodes. Additionally, the assembled Li_3YBr_6-based Li–S ASLIBs show good stability for up to 550 cycles. This work provides a reliable reference for the sustainable and environmentally friendly development of HSE-based ASLIBs.

Results and discussion

The phases of the as-prepared RE-based halides

VEA reaction equipment was used to synthesize and recover RE HSEs (Fig. 1a). A furnace heated flask is used to collect the as-

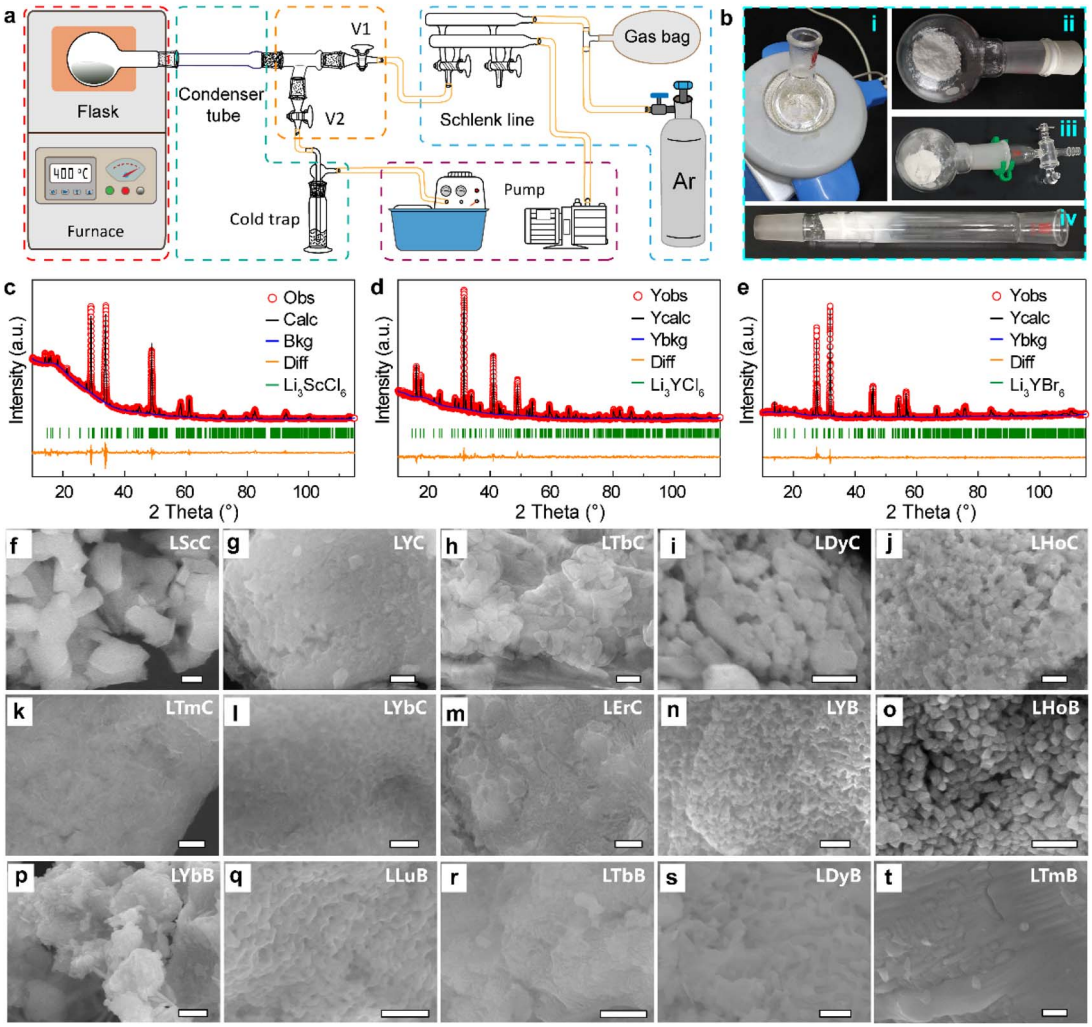

Fig. 1 Introduction of the VEA reactor, processes of the VEA reaction, and XRD patterns and SEM images of the as-synthesized HSEs. (a) Sketch map of the VEA reactor, including the heating zone (furnace and flask), condensing zone (condenser tube and cold trap), control valves, vacuum system (pump) and inert gas supply (Schlenk line, gas bag and Ar cylinder). (b) Pictures of the chemicals used during the VEA reaction: (i) solution of the raw materials in a quartz flask (100 mL), (ii) solid precursor powder, (iii) product and (iv) byproducts. (c–e) Rietveld refinement of the XRD patterns of LScC, LYC and LYB, respectively. (f–t) SEM images of LScC, LYC, LTbC, LDyC, LHoC, LTmC, LYbC, LErC, LYB, LHoB, LYbB, LLuB, LTbB, LDyB and LTmB; scale bar, 500 nm.

synthesized RE HSEs, and a condensing tube and cold trap are used to collect the by-products of solid NH_4X, and gas or liquid by-products, respectively. The Ar cylinder and Schlenk line supply inert gas, and the pumps provide a vacuum environment to remove O_2 and H_2O vapor. The dried precursor was obtained from a solution containing hydrous LiX, REX_3 and NH_4X, and the precursor can be further separated into Li_3REX_6, NH_4X (Fig. 1b), and other gaseous impurities. The X-ray diffraction (XRD) Rietveld refinement results of LScC, LYC and LYB show that they belong to monoclinic, hexagonal and monoclinic crystals, respectively (Fig. 1c–e and Tables S2, S3†). The XRD patterns of the as-synthesized hexagonal ($P\bar{3}m1$) Li_3YCl_6 (LYC), Li_3TbCl_6 (LTbC), Li_3DyCl_6 (LDyC), Li_3HoCl_6 (LHoC), Li_3ErCl_6 (LErC) and Li_3TmCl_6 (LTmC), orthorhombic (*Pnma*) Li_3YbCl_6 (LYbC), monoclinic ($C2/m$) Li_3ScCl_6 (LScC), Li_3YBr_6 (LYB), Li_3TbBr_6 (LTbB), Li_3DyBr_6 (LDyB), Li_3HoBr_6 (LHoB), Li_3TmBr_6 (LTmB), Li_3YbBr_6 (LYbB) and Li_3LuBr_6 (LLuB) are in good agreement with the standard PDF cards, except for LTmC, LTbB, LDyB and LTmB, which are symbiotic with a small amount of LiX or REX_3 (Fig. S1 and S2†). All these results show that most HSEs have been synthesized successfully. By using this method, RE halide perovskites, such as Cs_2NaYCl_6, Cs_2KYbCl_6, Na_3TbCl_6, Na_3YBr_6, Rb_3TbCl_6, Cs_3TbCl_6, $Cs_3Sc_2Cl_9$, $Cs_3Y_2Cl_9$, and $Cs_3Y_2Br_9$, can also be synthesized successfully (Fig. S3†).

The functions of ammonium halide in the VEA reaction

The addition of sufficient NH_4X is critical to the successful preparation of HSEs. The amount of NH_4X was 10 times more than that of RE ions in terms of the molar ratio during the preparation of anhydrous RE halides,[37] and enough NH_4X could produce HX gas to help decompose the oxygenated compounds and remove the impurities. The precursor powders of LYC (1-LYC, 2-LYC and 3-LYC precursors) and LYB (4-LYB, 5-LYB and 6-LYB precursors) contained LiX, YX_3, NH_4X and H_2O, and the molar ratios of NH_4X to YX_3 were 2.5, 5.0 and 20 (Fig. S4a and S4b†). After the reactions were finished, pure LYC (3-LYC product) and LYB (6-LYB product) were obtained from the precursor with 20 times NH_4X addition (Fig. S4c and S4d†). The insufficient addition of NH_4X is conducive to the formation of the impurities of LiX and RE oxyhalides (1-LYC, 2-LYC, 4-LYB and 5-LYB products). The by-products of NH_4X can be collected from the cold condenser (Fig. S4e and S4f†). In addition, the sublimation of NH_4X could generate abundant NH_3 and HX gases at high temperatures, which are conducive to the dispersion of metal halide salts and the formation of microscopic HSEs particles. Scanning electron microscopy (SEM) images showed that the morphologies of the HSEs varied from nanosized particles (LDyC, LHoC, LYB, LHoB, LLuB and LDyB) to porous structures (LYbC) and micron-sized blocks (LScC, LYC, LTbC, LTmC, LErC, LYbB, LTbB and LTmB), as shown in Fig. 1f–t. They include irregular micron-sized LScC, block LYC accumulated by various particles, irregular micron-sized LTbC lumps, non-uniform nano- and micron-sized LDyC particles, nanosized particles and micron sized blocks of LHoC, block LTmC with a rough surface, porous structure aggregation LYbC with nanosized particles, block LErC with a rough surface and irregular cracks, adhered LYB nanoparticles, uniform LHoB nanoparticles, irregular LYbB nanoparticles and microparticles, adhered LLuB nanoparticles, non-uniform LTbB particles, adhered LDyB nanoparticles, and LTmB blocks with cracks and particles on the surface. The different crystallization points of the HSEs lead to various morphologies under the same reaction conditions. The results show that the morphologies and sizes of RE HSEs could be controlled by adjusting the amount of NH_4X, heating rate and temperature during the reaction. The SEM energy dispersive spectrometer results revealed that both RE and halogen were evenly distributed with no obvious aggregation, and the content ratio of RE and halogen was consistent with that of the stoichiometry of each HSEs (Fig. S5–S19†).

Closed-loop cycle routes of RE, lithium and ammonium salts

The traditional (black line) and new (red line) cycle lines of lithium, RE and other chemicals during the application of HSEs are shown in Fig. 2. The traditional chemical process of HSEs preparation and recycling must start and end with the consumption and production of anhydrous halides (LiX and REX_3) because the oxy compounds of RE and lithium cannot be used as raw materials in ball-milling and co-melting methods. The VEA reactor plays a major role in the preparation, recovery and recycling of HSEs. The VEA reactor can decompose RE and lithium based raw materials (RE_2O_3, $RE_2(CO_3)_3$, Li_2CO_3, *etc.*) into various products and distribute the products to separate cycling paths of RE and lithium (red line), NH_4X (blue line), and H_2O or CO_2 (green line). Because of their strong hydrophilicity, HSEs can absorb H_2O forming oxygenated metal compounds, and further to produce RE oxyhalides or other metal chemicals. As long as the molar ratio of lithium to RE in the raw materials is 3/1, the HSEs can be produced by the VEA reactor in one step, which greatly improves the efficiency of recovery and cycling of HSEs from deteriorated or recycled HSEs. As an example, the degraded LYC and LYB can be recovered to pure phases (Fig. 3a and b). As the auxiliary reagent, NH_4X helps to remove oxygen-related impurities during the VEA reaction, and the average recovery rate of condensed NH_4X was more than 97% without the addition of the lost parts in the collection process (Table S4†). The collected NH_4X can be reused in the VEA reaction or serve as useful chemicals in other fields. The produced CO_2 can be collected and used in the process of metal extraction. Ultimately, the RE and Li resources, and the nitrogen- and carbon-related chemicals finished their respective closed-loop circulations. During the processes of massive HSEs preparation, the precursors, products and byproducts can be easily obtained and collected (Fig. S20†).

Massive amounts of LScC (~27.5 g), LYC (~32.0 g), LYB (~58.5 g) and LHoB (~65.9 g) were successfully prepared (yield, >99%) (Fig. 3c–f). The formation of RE HSEs in the VEA reaction can be expressed by eqn (11) with the help of an auxiliary reagent of NH_4X. Similarly, the deliquescence (eqn (12)), degradation (eqn (13)) and recovery (eqn (14) and (15)) of HSEs can be expressed by different chemical reaction equations. In addition, RE HSEs can be synthesized in one step from the

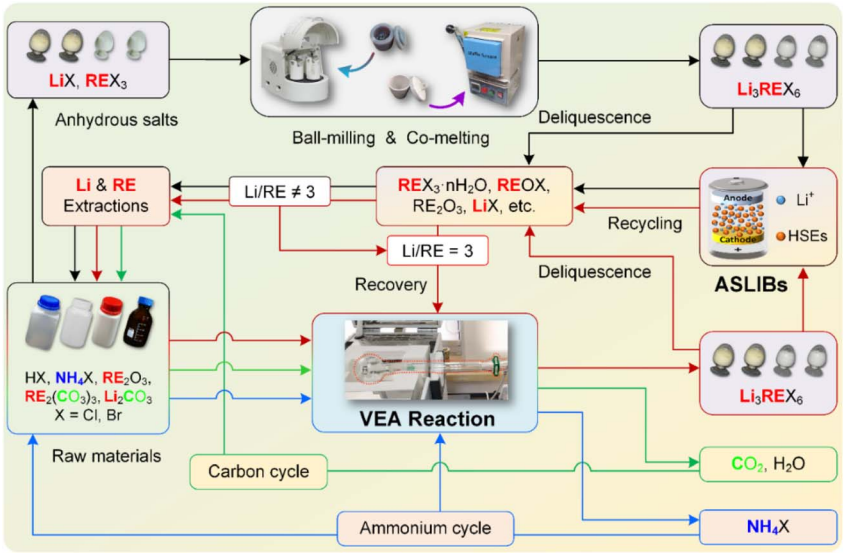

Fig. 2 Schematic diagram of the cycle routes of RE HSEs. The closed cycles of RE elements, lithium, ammonium halides and CO_2 throughout the processes of RE HSEs production, utilization and recycling. The black line represents the cycle path of the HSEs by mechanochemical BM and the high-temperature CM methods. Red line, the cycle routes of HSEs and the related metal-based chemicals through the VEA reactor. The green line represents the closed cycle of CO_2 and H_2O. The blue line represents the closed cycle of NH_4X during the VEA reaction process.

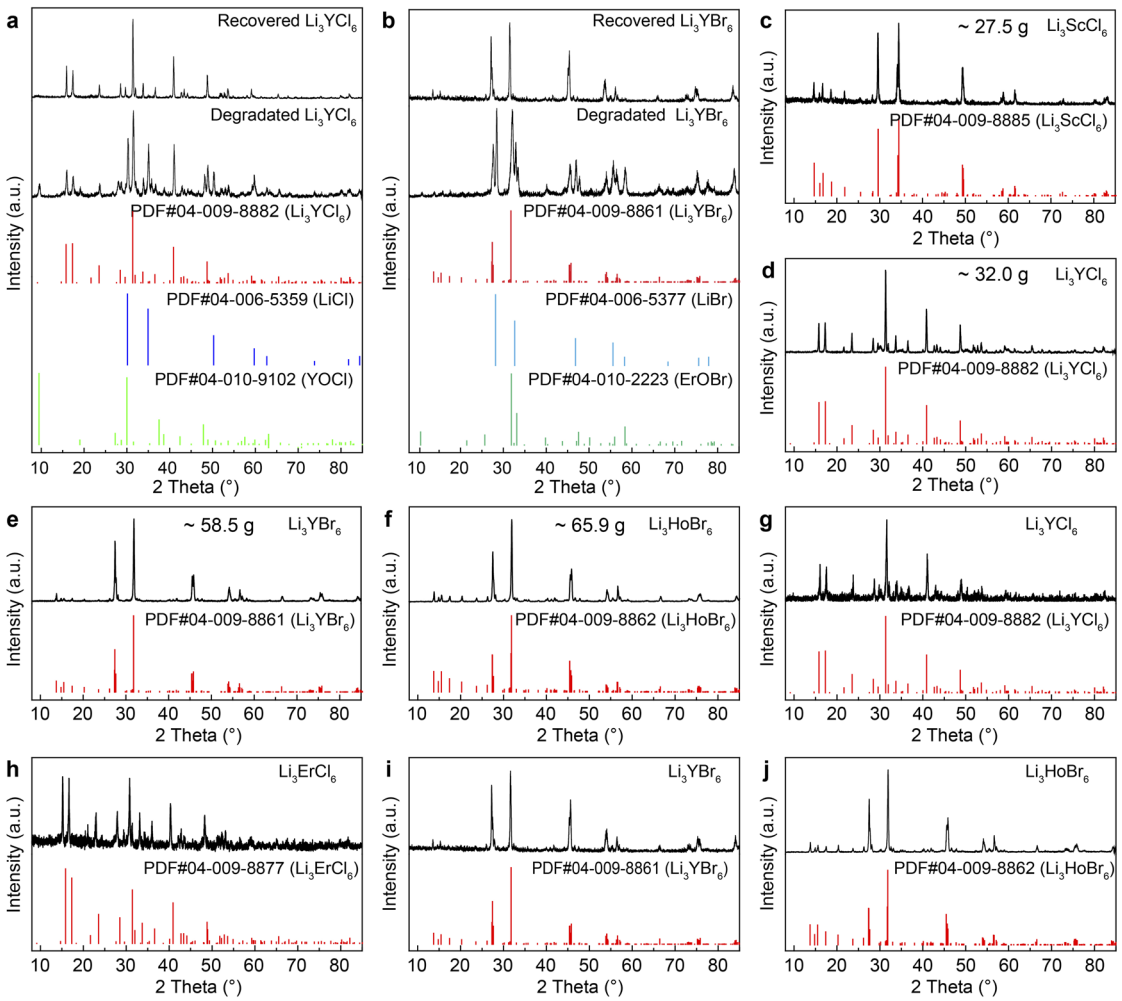

Fig. 3 XRD patterns of the recovered, massively synthesized and solvent-free prepared HSEs by the VEA method. (a) The degraded and recovered LYC. (b) The degraded and recovered LYB. (c–f) Massively synthesized LScC, LYC, LYB and LHoB. (g–j) Solvent-free synthesized LYC, LErC, LYB and LHoB from RE oxides and lithium carbonate.

solvent-free reaction of heating the mixture of RE oxides, Li_2CO_3 and sufficient NH_4X in the VEA reactor (eqn (16)). The decomposable NH_4X could provide halogen anions to combine with metal ions forming HSEs, and the gaseous byproducts of NH_3, CO_2 and H_2O produced at high temperature could be removed. Therefore, pure LYC, LErC, LYB and LHoB can be synthesized successfully from metal oxygen-containing compounds (Fig. 3g–j).

$$RE_2O_3 + 3Li_2CO_3 + 12HX \xrightarrow{\Delta/NH_4X} 2Li_3REX_6 + 6H_2O\uparrow + 6CO_2\uparrow \quad (11)$$

$$Li_3REX_6 + (3m + n)H_2O \rightarrow 3LiX{\cdot}mH_2O + REX_3{\cdot}nH_2O \quad (12)$$

$$REX_3{\cdot}nH_2O + 3LiX{\cdot}mH_2O \xrightarrow{\Delta} REOX + 3LiX + (3m + n - 1)H_2O\uparrow + 2HX\uparrow \quad (13)$$

$$3LiX + REOX + 2HX \xrightarrow{\Delta/NH_4X} Li_3REX_6 + H_2O\uparrow \quad (14)$$

$$3LiX + REOX + 2NH_4X \xrightarrow{\Delta/NH_4X} Li_3REX_6 + H_2O\uparrow + 2NH_3\uparrow \quad (15)$$

$$RE_2O_3 + 3Li_2CO_3 + 12NH_4X \xrightarrow{\Delta/NH_4X} 2Li_3REX_6 + 6H_2O\uparrow + 3CO_2\uparrow + 12NH_3\uparrow \quad (16)$$

Electrochemical properties of the prepared HSEs

The as-prepared RE HSEs have excellent formability and can be formed into compacted electrolyte pellets by cold pressing. The lithium ion (Li^+) conductivities of the HSEs were calculated from the Nyquist plots of the electrochemical impedance spectroscopy (EIS) on In/HSEs/In (In, indium metal) cells at room temperature (RT) (Fig. 4a and S21†). The results show that

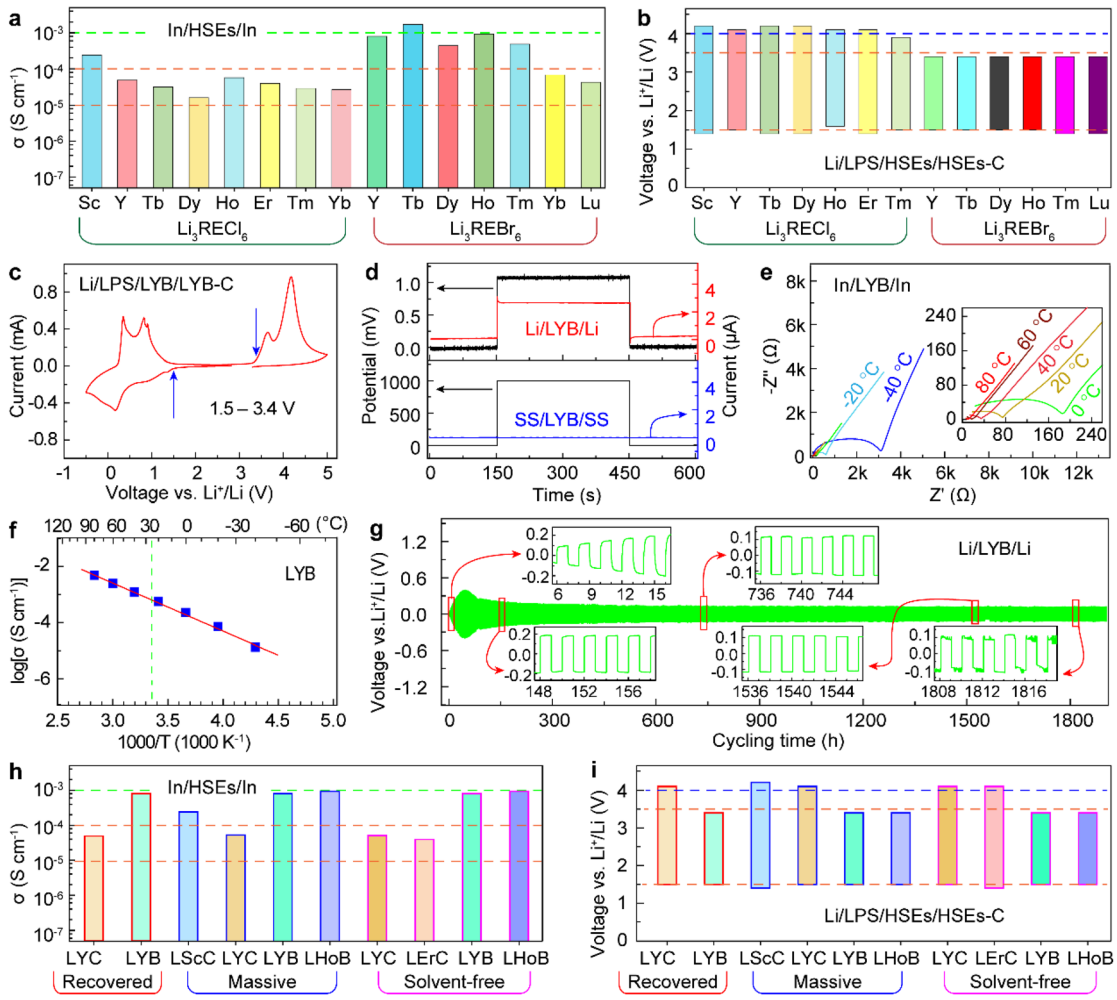

Fig. 4 The electrochemical performance of the HSEs prepared by the VEA method. (a) Li ion conductivities of the as-synthesized Li_3RECl_6 and Li_3REBr_6. (b) Electrochemical windows of as-synthesized Li_3RECl_6 and Li_3REBr_6. (c) Cyclic voltammetry curve of the Li/LPS/LYB/LYB–C battery (−0.5 to 5.0 V, 0.5 mV s^{-1}). (d) The transient current behavior of LYB, Li metal and SG acting as reversible and irreversible electrodes, respectively. (e) Nyquist plots of LYB at different temperatures (−40 to 80 °C). (f) Arrhenius conductivity plot of LYB. (g) Cycle stability of the Li/LYB/Li symmetric cell (0.1 mA cm^{-2}). (h) Li ion conductivities of the recovered, massively synthesized and solvent-free prepared HSEs. (i) Electrochemical windows of the recovered, massively synthesized and solvent-free prepared HSEs.

the HSEs synthesized by the VEA reactor have high Li^+ conductivities and that bromide SEs have higher Li^+ conductivities than that of the chloride SEs (Table S5†). LScC has a higher Li^+ conductivity (0.24 mS cm^{-1}) than LYC (0.049 mS cm^{-1}), LTbC (0.032 mS cm^{-1}), LDyC (0.016 mS cm^{-1}), LHoC (0.057 mS cm^{-1}), LErC (0.04 mS cm^{-1}), LTmC (0.029 mS cm^{-1}) and LYbC (0.027 mS cm^{-1}). LTbB has a higher ionic conductivity of up to 1.7 mS cm^{-1} than LYB (0.8 mS cm^{-1}), LDyB (0.44 mS cm^{-1}), LHoB (0.93 mS cm^{-1}), LTmB (0.48 mS cm^{-1}), LYbB (0.068 mS cm^{-1}) and LLuB (0.043 mS cm^{-1}). The electrochemical windows of the HSEs were obtained from the cyclic voltammograms of Li/LPS/HSEs/HSEs-C cells (Fig. 4b, c and S22†).[42] The results show that all of the prepared HSEs have good electrochemical stability and that Li_3RECl_6 has a wider electrochemical window (1.4–4.2 V, *vs.* Li/Li^+) than Li_3REBr_6 (1.5–3.4 V) (Table S5†).

Among these RE HSEs, the raw materials of LYC and LYB are the cheapest, and yttrium is abundant in the crust.[43] Therefore, it is necessary to study the performance and applications of LYC and LYB in ASLIBs, which are important for the industrialization and sustainable development of ASLIBs. The symmetric Li/LYB/Li cell and SG/LYB/SG (SG, stainless-steel gasket) blocking cell showed that LYB is Li^+ conductive with an external bias voltage of 1 mV and electrical insulation applied at a higher voltage of 1000 mV (Fig. 4d). The temperature-dependent Nyquist plots of the In/LYB/In cells revealed that the ionic conductivity of LYB increased with increasing temperature from −40 °C to 80 °C (Fig. 4e). The calculated activation energy of LYB is 0.34 eV (lower than 0.5 eV) from the Arrhenius

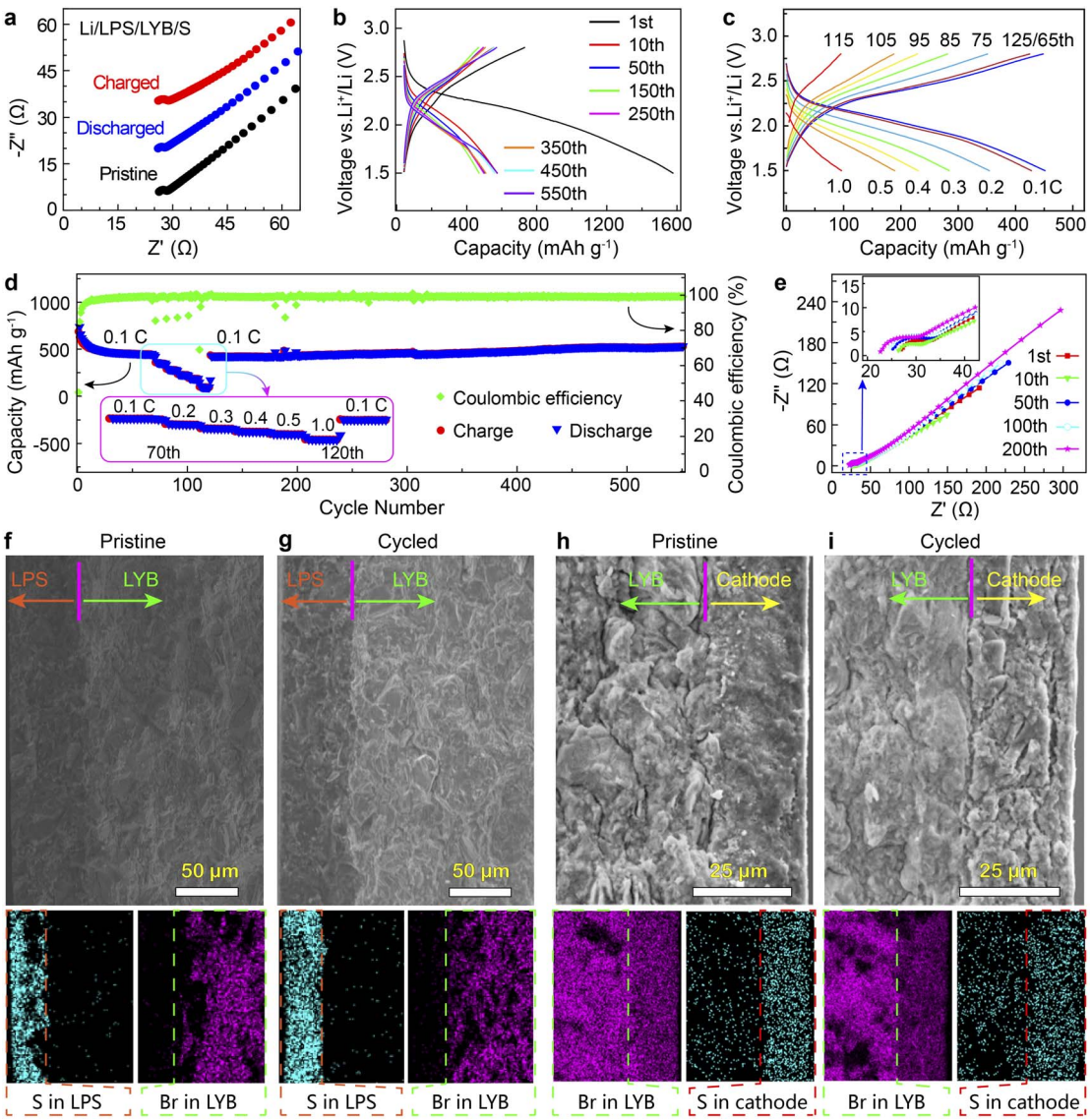

Fig. 5 The electrochemical performance of the Li/LPS/LYB/S battery. (a) Nyquist plots of the battery during the process of charging and discharging. (b) Galvanostatic charge–discharge curves at various cycles. (c) Charge–discharge curves with different rates and cycles. (d) Cycle stability and rate capability. (e) Nyquist plots of the battery after cycling for different times. (f–i) Cross-sectional SEM images and corresponding EDS maps of the pristine and cycled cells at the LPS/LYB and LYB/S interfaces.

conductivity plot (Fig. 4f), indicating that LYB has good Li ion migration capacity over a wide temperature range. A symmetric Li/LYB/Li cell was used to evaluate the stability of LYB with the Li anode. Y^{3+} could be reduced by Li metal at the interface of Li and LYB because of the lower electrode potential of Li^+/Li (−3.04 V) than that of Y^{3+}/Y (−2.37 V).[44–46] Thus, the voltage increased in the initial state (first to 40 cycles) and then decreased and stabilized up to 1540 cycles (Fig. 4g). After that, a voltage fluctuation was observed, which shows the long-term instability of the interface of Li and LYB. Importantly, the electrochemical properties of the recovered, massive synthesized and solvent-free prepared HSEs are consistent without performance degradation (Fig. 4h, i, S23–S26 and Table S6†).

The performance of the Li/LPS/LYB/S solid battery

To ensure that the ASLIBs had long cycles, LPS was used as a buffer layer between Li and LYB to stabilize its interface.[47] It is also necessary to avoid irreversible redox reactions between the cathode and SEs.[48–51] Therefore, the sulfur-containing composite cathode was used directly to assemble all solid Li–S button batteries Li/LPS/LYB/S. The cycling voltammetry (CV) curves (0.1 mV s^{-1}, 1.0–3.0 V) of the Li/LPS/LYB/S battery at different cycles cannot overlap well, which also corresponds to the low initial Coulombic efficiency (CE) (Fig. S27†). The Nyquist plots of the discharged and charged batteries showed a small internal impedance of approximately 28 Ω (Fig. 5a). This finding proved that the electrodes (Li and S) and electrolytes (LPS and LYB) can guarantee the efficient transfer of electrons and Li^+.

The first charge–discharge curves revealed that the CE of the Li/LPS/LYB/S battery is low (45%), maintaining steady work from the 10th to 550th cycles (Fig. 5b), which is related to the S cathode volume expansion and incomplete oxidation of Li_2S in the initial state.[52,53] The battery can maintain normal charge–discharge (Fig. 5c), and it has a stable capacity for up to 550 cycles and a high CE of nearly 100% after charging and discharging at different rates (1.0C = 1675 mA g^{-1}) (Fig. 5d). The Nyquist plots of the cycled battery at different times show that the impedance of the battery does not change significantly (Fig. 5e). The cross-sectional SEM images and EDS maps of S and Br inside the battery showed that the thickness of the LPS did not change significantly after cycling (Fig. 5f and g), indicating that the LPS buffer layer between Li and LYB was stable during the cycling process. SEM images and EDS mapping of S and Br show that the thickness of the cathode (S) increased after cycling, which was due to the expansion of Li_2S formation (Fig. 5h and i).[54] In addition, LYB was used in the Li–In/LPS/LYB/LTO ($Li_4Ti_5O_{12}$) battery, which can realize reversible capacity (0.1C, 151 mA h g^{-1}, ∼86% of theoretical value), long-term stability for 7500 cycles at high current density (10.0C, 1.0C = 175 mA g^{-1}) and high CE close to 100% (Fig. S28†).

Conclusions

This work provides an efficient and convenient method to synthesize RE HSEs and RE halide perovskites from inexpensive RE compounds. The raw materials, products and by-products can be well arranged in various closed-loop circulation paths without pollution emissions during the VEA reactor. This method provides a technical reference for the massive preparation, recovery and recycling of RE HSEs in the ASLIB industry. The synthesized HSEs showed excellent performance with high ionic conductivity (∼1 mS cm^{-1}) and stable electrochemical windows (1.4–4.2 V). The LYB based solid Li–S battery can work stably for 550 cycles without obvious capacity fading, and the CE is close to 100%. This method can be applied to prepare and recycle other RE-based halide functional materials, and it is highly important for the sustainable development of energy-related precious metal resources.

Data availability

The data supporting this article have been included as part of the ESI.†

Author contributions

Y. P. Du supervised the research. Z. C. Zeng conceived the concept, performed the experiments, and wrote the manuscript. X. M. Shi, and H. T. Zhang fabricated and tested the solid batteries. All the authors participated in the data analysis and manuscript discussion.

Conflicts of interest

There are no conflicts to declare.

Acknowledgements

We gratefully acknowledge the support from the National Science Foundation for Distinguished Young Scholars of China (22425503), National Natural Science Foundation of China (22371131, 22305129), the 111 Project (B18030) from China, Tianjin Natural Science Foundation (24JCQNJC01980), the Key Laboratory of Rare Earths, Chinese Academy of Sciences, the China Postdoctoral Science Foundation (BX20220157, 2022M721698, 2023M741812), and Rare Earth Advanced Materials Technology Innovation Center.

References

1 Y. Chen, Z. Lun, X. Zhao, K. P. Koirala, L. Li, Y. Sun, C. A. O'Keefe, X. Yang, Z. Cai, C. Wang, H. Ji, C. P. Grey, B. Ouyang and G. Ceder, Unlocking Li superionic conductivity in face-centred cubic oxides via face-sharing configurations, *Nat. Mater.*, 2024, **23**, 535–542.

2 X. Li, J. Kim, J. Luo, C. Zhao, Y. Xu, T. Mei, R. Li, J. Liang and X. Sun, Structural regulation of halide superionic conductors for all-solid-state lithium batteries, *Nat. Commun.*, 2024, **15**, 53.

3 Q. Zhao, S. Stalin, C. Zhao and L. Archer, Designing solid-state electrolytes for safe, energy-dense batteries, *Nat. Rev. Mater.*, 2020, **5**, 229–252.

4 L. Jia, J. Zhu, X. Zhang, B. Guo, Y. Du and X. Zhuang, Li–solid electrolyte interfaces/interphases in all-solid-state Li batteries, *Electrochem. Energy Rev.*, 2024, **7**, 12.
5 R. Chen, Q. Li, X. Yu, L. Chen and H. Li, Approaching practically accessible solid-state batteries: Stability issues related to solid electrolytes and interfaces, *Chem. Rev.*, 2020, **120**, 6820–6877.
6 G. Han, A. Vasylenko, L. M. Daniels, C. M. Collins, L. Corti, R. Chen, H. Niu, T. D. Manning, D. Antypov, M. S. Dyer, J. Lim, M. Zanella, M. Sonni, M. Bahri, H. Jo, Y. Dang, C. M. Robertson, F. Blanc, L. J. Hardwick, N. D. Browning, J. B. Claridge and M. J. Rosseinsky, Superionic lithium transport via multiple coordination environments defined by two-anion packing, *Science*, 2024, **383**, 739–745.
7 P. Lu, Z. Zhou, Z. Xiao, J. Lu, J. Zhang, G. Hu, W. Yan, S. Xia, S. Zhang, Z. Wang, H. Li, C. Wang, F. Wu and X. Sun, Materials and chemistry design for low-temperature all-solid-state batteries, *Joule*, 2024, **8**, 635–657.
8 J. Liang, X. Li, K. Adair and X. Sun, Metal halide superionic conductors for all-solid-state batteries, *Acc. Chem. Res.*, 2021, **54**, 1023–1033.
9 Y. Yin, J. Yang, J. Luo, G. Lu, Z. Huang, J. Wang, P. Li, F. Li, Y. Wu, T. Tian, Y. Meng, H. Mo, Y. Song, J. Yang, L. Feng, T. Ma, W. Wen, K. Gong, L. Wang, H. Ju, Y. Xiao, Z. Li, X. Tao and H. Yao, A $LaCl_3$-based lithium superionic conductor compatible with lithium metal, *Nature*, 2023, **616**, 77–83.
10 S. Yu, J. Noh, B. Kim, J.-H. Song, K. Oh, J. Yoo, S. Lee, S.-O. Park, W. Kim, B. Kang, D. Kil and K. Kang, Design of a trigonal halide superionic conductor by regulating cation order-disorder, *Science*, 2023, **382**, 573–579.
11 Q. Wang, Y. Zhou, X. Wang, H. Guo, S. Gong, Z. Yao, F. Wu, J. Wang, S. Ganapathy, X. Bai, B. Li, C. Zhao, J. Janek and M. Wagemaker, Designing lithium halide solid electrolytes, *Nat. Commun.*, 2024, **15**, 1050.
12 X. Li, J. Liang, X. Yang, K. Adair, C. Wang, F. Zhao and X. Sun, Progress and perspectives on halide lithium conductors for all-solid-state lithium batteries, *Energy Environ. Sci.*, 2020, **13**, 1429–1461.
13 L. M. Wang, W. Xiao, L. Sun, R. Yang, J. Q. Yu and L. G. Wang, Atomistic mechanism of high ionic conductivity in lithium ytterbium-based halide solid electrolytes: A first-principles study, *J. Rare Earths*, 2024, **42**, 155–162.
14 J. Wu, J. Li and X. Yao, Exploring the potential of halide electrolytes for next-generation all-solid-state lithium batteries, *Adv. Funct. Mater.*, 2025, **35**, 2416671.
15 R. Schlem, S. Muy, N. Prinz, A. Banik, Y. Shao-Horn, M. Zobel and W. Zeier, Mechanochemical synthesis: A tool to tune cation site disorder and ionic transport properties of Li_3MCl_6 (M = Y, Er) superionic conductors, *Adv. Energy Mater.*, 2019, **10**, 1903719.
16 L. Zhou, C. Kwok, A. Shyamsunder, Q. Zhang, X. Wu and L. Nazar, A new halospinel superionic conductor for high-voltage all solid state lithium batteries, *Energy Environ. Sci.*, 2020, **13**, 2056–2063.
17 X. Shi, Z. Zeng, H. Zhang, B. Huang, M. Sun, H. Wong, Q. Lu, W. Luo, Y. Huang, Y. Du and C. Yan, Gram-scale synthesis of nanosized Li_3HoBr_6 solid electrolyte for all-solid-state Li-Se battery, *Small Methods*, 2021, **5**, 2101002.
18 B. He, F. Zhang, Y. Xin, C. Xu, X. Hu, X. Wu, Y. Yang and H. Tian, Halogen chemistry of solid electrolytes in all-solid-state batteries, *Nat. Rev. Chem*, 2023, **7**, 826–842.
19 T. Asano, A. Sakai, S. Ouchi, M. Sakaida, A. Miyazaki and S. Hasegawa, Solid halide electrolytes with high lithium-ion conductivity for application in 4 V class bulk-type all-solid-state batteries, *Adv. Mater.*, 2018, **30**, 1803075.
20 H. Kwak, D. Han, J. Lyoo, J. Park, S. Jung, Y. Han, G. Kwon, H. Kim, S. Hong, K. Nam and Y. Jung, New cost-effective halide solid electrolytes for all-solid-state batteries: Mechanochemically prepared Fe^{3+}-substituted Li_2ZrCl_6, *Adv. Energy Mater.*, 2021, **11**, 2003190.
21 M. Ziegler and J. Trancik, Re-examining rates of lithium-ion battery technology improvement and cost decline, *Energy Environ. Sci.*, 2021, **14**, 1635–1651.
22 J. Schnell, F. Tietz, C. Singer, A. Hofer, N. Billot and G. Reinhart, Prospects of production technologies and manufacturing costs of oxide-based all-solid-state lithium batteries, *Energy Environ. Sci.*, 2019, **12**, 1818–1833.
23 K. Tuo, C. Sun and S. Liu, Recent progress in and perspectives on emerging halide superionic conductors for all-solid-state batteries, *Electrochem. Energy Rev.*, 2023, **6**, 17.
24 R. Herrington, Mining our green future, *Nat. Rev. Mater.*, 2021, **6**, 456–458.
25 X. Ma, L. Azhari and Y. Wang, Li-ion battery recycling challenges, *Chem*, 2021, **7**, 1–5.
26 C. Bauer, S. Burkhardt, N. P. Dasgupta, L. A.-W. Ellingsen, L. L. Gaines, H. Hao, R. Hischier, L. Hu, Y. Huang, J. Janek, C. Liang, H. Li, J. Li, Y. Li, Y.-C. Lu, W. Luo, L. F. Nazar, E. A. Olivetti, J. F. Peters, J. L. M. Rupp, M. Weil, J. F. Whitacre and S. Xu, Charging sustainable batteries, *Nat. Sustain.*, 2022, **5**, 176–178.
27 J. Wang, J. Ma, Z. Zhuang, Z. Liang, K. Jia, G. Ji, G. Zhou and H. Cheng, Toward direct regeneration of spent lithium-ion batteries: A next-generation recycling method, *Chem. Rev.*, 2024, **124**, 2839–2887.
28 M. Ahuis, S. Doose, D. Vogt, P. Michalowski, S. Zellmer and A. Kwade, Recycling of solid-state batteries, *Nat. Energy*, 2024, **9**, 373–385.
29 J. Zimmerman, P. Anastas, H. Erythropel and W. Leitner, Designing for a green chemistry future, *Science*, 2020, **367**, 397–400.
30 S. Dühnen, J. Betz, M. Kolek, R. Schmuch, M. Winter and T. Placke, Toward green battery cells: Perspective on materials and technologies, *Small Methods*, 2020, **4**, 2000039.
31 K. Binnemans, P. McGuiness and P. Jones, Rare-earth recycling needs market intervention, *Nat. Rev. Mater.*, 2021, **6**, 459–461.
32 Z. Yang, F. Xiao, S. Sun, H. Zhong and G. Tu, REEs recovery from molten salt electrolytic slag: Challenges and opportunities for environmentally friendly techniques, *J. Rare Earths*, 2024, **42**, 1009–1019.

33 D. Yang, M. Yu, Y. Mubula, W. Yuan, Z. Huang, B. Lin, G. Mei and T. Qiu, Recovering rare earths, lithium and fluorine from rare earth molten salt electrolytic slag using sub-molten salt method, *J. Rare Earths*, 2024, **42**, 1774–1781.

34 J. Miller, S. Miller and R. Himes, Preparation of anhydrous rare earth chlorides for physicochemical studies, *J. Am. Chem. Soc.*, 1959, **81**, 4449–4451.

35 J. Yu, P. Peng, C. Diao, H. Wu and H. He, Preparation and characterization of high purity anhydrous rare earth halides for scintillation crystal growth, *J. Synth. Cryst.*, 2016, **45**, 321–327.

36 J. Xiao, C. Chen, W. Ding, Y. Peng, K. Zou, T. Chen and Z. Zou, Preparing high-purity anhydrous $ScCl_3$ molten salt using one-step rapid heating process, *Appl. Sci.*, 2020, **10**, 5174.

37 M. Taylor and C. Carter, Preparation of anhydrous lanthanide halides, especially iodides, *J. Inorg. Nucl. Chem.*, 1962, **24**, 387–391.

38 B. Kubikova, L. Rycerz, I. Chojnacka and M. Gaune-Escard, Phase diagram and thermodynamic and transport properties of the $DyBr_3$-LiBr binary system, *J. Phase Equilib. Diffus.*, 2009, **30**, 502–508.

39 S. Muy, J. Voss, R. Schlem, R. Koerver, S. Sedlmaier, F. Maglia, P. Lamp, W. Zeier and Y. Shao-Horn, High-throughput screening of solid-state Li-ion conductors using lattice-dynamics descriptors, *iScience*, 2019, **16**, 270–282.

40 J. Liang, X. Li, S. Wang, K. Adair, W. Li, Y. Zhao, C. Wang, Y. Hu, L. Zhang, S. Zhao, S. Lu, H. Huang, R. Li, Y. Mo and X. Sun, Site-occupation-tuned superionic Li_xScCl_{3+x} halide solid electrolytes for all-solid-state batteries, *J. Am. Chem. Soc.*, 2020, **142**, 7012–7022.

41 L. Zhou, T.-T. Zuo, C. Y. Kwok, S. Y. Kim, A. Assoud, Q. Zhang, J. Janek and L. F. Nazar, High areal capacity, long cycle life 4 V ceramic all-solid-state Li-ion batteries enabled by chloride solid electrolytes, *Nat. Energy*, 2022, **7**, 83–93.

42 W. Ji, D. Zheng, X. Zhang, T. Ding and D. Qu, A kinetically stable anode interface for Li_3YCl_6-based all-solid-state lithium batteries, *J. Mater. Chem. A*, 2021, **9**, 15012–15018.

43 K. Wang, Q. Ren, Z. Gu, C. Duan, J. Wang, F. Zhu, Y. Fu, J. Hao, J. Zhu, L. He, C. Wang, Y. Lu, J. Ma and C. Ma, A cost-effective and humidity-tolerant chloride solid electrolyte for lithium batteries, *Nat. Commun.*, 2021, **12**, 4410.

44 C. Wang, J. Liang, J. Luo, J. Liu, X. Li, F. Zhao, R. Li, H. Huang, S. Zhao, L. Zhang, J. Wang and X. Sun, A universal wet-chemistry synthesis of solid-state halide electrolytes for all-solid-state lithium-metal batteries, *Sci. Adv.*, 2021, **7**, eabh1896.

45 H. Zhao, J. Xia, D. Yin, M. Luo, C. Yan and Y. Du, Rare earth incorporated electrode materials for advanced energy storage, *Coord. Chem. Rev.*, 2019, **390**, 32–49.

46 L. Riegger, R. Schlem, J. Sann, W. Zeier and J. Janek, Lithium-metal anode instability of the superionic halide solid electrolytes and the implications for solid-state batteries, *Angew. Chem., Int. Ed.*, 2021, **60**, 6718–6723.

47 J. Wu, S. Liu, F. Han, X. Yao and C. Wang, Lithium/sulfide all-solid-state batteries using sulfide electrolytes, *Adv. Mater.*, 2021, **33**, 2000751.

48 D. Park, H. Park, Y. Lee, S. Kim, H. Jung, K. Chung, J. Shim and S. Yu, Theoretical design of lithium chloride superionic conductors for all-solid-state high-voltage lithium-ion batteries, *ACS Appl. Mater. Interfaces*, 2020, **12**, 34806–34814.

49 G. Chun, J. Shim and S. Yu, Computational investigation of the interfacial stability of lithium chloride solid electrolytes in all-solid-state lithium batteries, *ACS Appl. Mater. Interfaces*, 2022, **14**, 1241–1248.

50 X. Shi, Z. Zeng, H. Zhang, Y. Huang, C. H. Yan and Y. Du, Encapsulating and operating a stable Li_3ErBr_6-based solid Li-SeS_2 battery at room temperature, *Adv. Funct. Mater.*, 2023, **33**, 2213638.

51 Z. Wang, J. Xia, X. Ji, Y. Liu, J. Zhang, X. He, W. Zhang, H. Wan and C. Wang, Lithium anode interlayer design for all-solid-state lithium-metal batteries, *Nat. Energy*, 2024, **9**, 251–262.

52 X. Xu, Y. Liu, O. Kapitanova, Z. Song, J. Sun and S. Xiong, Electro–chemo–mechanical failure of solid electrolytes induced by growth of internal lithium filaments, *Adv. Mater.*, 2022, **34**, 2207232.

53 S. Kalnaus, N. J. Dudney, A. S. Westover, E. Herbert and S. Hackney, Solid-state batteries: The critical role of mechanics, *Science*, 2023, **381**, eabg5998.

54 S. Ohno, R. Koerver, G. Dewald, C. Rosenbach, P. Titscher, D. Steckermeier, A. Kwade, J. Janek and W. Zeier, Observation of chemomechanical failure and the influence of cutoff potentials in all-solid-state Li-S batteries, *Chem. Mater.*, 2019, **31**, 2930–2940.